Naval Research Laboratory
Washington, DC 20375-5320

NRL/MR/6410--05-8905

Computational Fluid Dynamics Study for Optimization of a Fin Design

RAVI RAMAMURTI
WILLIAM C. SANDBERG

Center for Reactive Flow and Dynamical Systems
Laboratory for Computational Physics and Fluid Dynamics

September 28, 2005

REPORT DOCUMENTATION PAGE

Form Approved
OMB No. 0704-0188

1. REPORT DATE *(DD-MM-YYYY)*	2. REPORT TYPE	3. DATES COVERED *(From - To)*
28-09-2005	Memorandum Report	

4. TITLE AND SUBTITLE

Computational Fluid Dynamics Study for Optimization of a Fin Design

5a. CONTRACT NUMBER

5b. GRANT NUMBER
64-6093-A-5

5c. PROGRAM ELEMENT NUMBER

6. AUTHOR(S)

Ravi Ramamurti and William C. Sandberg

5d. PROJECT NUMBER

5e. TASK NUMBER

5f. WORK UNIT NUMBER

7. PERFORMING ORGANIZATION NAME(S) AND ADDRESS(ES)

Naval Research Laboratory, Code 6410
4555 Overlook Avenue, SW
Washington, DC 20375-5320

8. PERFORMING ORGANIZATION REPORT NUMBER

NRL/MR/6410--05-8905

9. SPONSORING / MONITORING AGENCY NAME(S) AND ADDRESS(ES)

10. SPONSOR / MONITOR'S ACRONYM(S)

11. SPONSOR / MONITOR'S REPORT NUMBER(S)

12. DISTRIBUTION / AVAILABILITY STATEMENT

Approved for public release; distribution is unlimited.

13. SUPPLEMENTARY NOTES

14. ABSTRACT

The three-dimensional, unsteady computations of an Unmanned Underwater vehicle with flapping fins were carried out. Several parametric studies were performed varying the amplitude and frequency of oscillation of the fin and the angle of attack of the fin at the root. The objective of these computations was to investigate the importance of these parameters on the fluid dynamics of force production in order to propel the vehicle at a constant speed of 3 kt. An unstructured grid-based unsteady Navier-Stokes solver with automatic adaptive remeshing was used to compute the flow about the vehicle through several complete cycles of fin oscillation for each of the cases studied. The computations show that the angle of attack of 20° of the root section of the fin is near optimum. The vehicle is capable of sustaining a 3 kt current and maintaining position with the fins flapping at a frequency of 2 Hz and an amplitude of 114°. As the frequency of oscillation is increased, the net thrust produced increases, but the vehicle will be subjected to large excursions in the normal force. As the fin is made rigid, there is a substantial penalty in lift during the upstroke.

15. SUBJECT TERMS

Flapping foil; Deforming fin; Incompressible flow; Unstructured grid

16. SECURITY CLASSIFICATION OF:			17. LIMITATION OF ABSTRACT	18. NUMBER OF PAGES	19a. NAME OF RESPONSIBLE PERSON
a. REPORT	b. ABSTRACT	c. THIS PAGE			Ravi Ramamurti
Unclassified	Unclassified	Unclassified	UL	16	19b. TELEPHONE NUMBER *(include area code)* (202) 767-0608

Table of Contents

List of Figures

Computational Fluid Dynamics Study for Optimization of a Fin Design

INTRODUCTION

Many fishes that swim with paired pectoral fins use fin stroke parameters that produce thrust force from lift in powering their underwater flight. Flapping locomotion mechanisms are of interest to behavioral biologists, biomechanics researchers, and engineers attempting to develop systems that can match the performance of the living creatures. One question that arises in investigating the mechanisms responsible for the high thrust/lift generation in flapping locomotion is the importance of chordwise and spanwise deformation. Flapping foil propulsion has also received considerable attention in the past few years as an alternative to the propeller. This mode of propulsion which involves no body undulation, has many applications, such as submersibles propulsion, maneuvering, position-keeping and flow control which are of interest to the Unmanned Underwater Vehicle (UUV) hydrodynamic community and unconventional aerodynamics of Micro Aerial Vehicles (MAV) for the aerodynamic community. For both types of vehicles, it is important to accurately quantify the performance benefits of flexible wings, since providing the flexibility is a major technical challenge.

Dickinson et al. (1999) has studied the effects of the wing rotation in the fruitfly, *Drosophila,* and Walker and Westneat (1997) have studied the kinematics of the fin motion in a class of fishes, namely the bird wrasse, experimentally. Three dimensional unsteady flow computations over insects have been carried out by Liu and Kawachi (1998) who obtained qualitative agreement for the flow patterns over a hovering hawkmoth with the windtunnel visualizations of Willmott and Ellington (1997). Ramamurti and Sandberg have studied the force production in *Drosophila* (2002a) and in a swimming bird wrasse fish (2002b) computationally and obtained good agreement with experimental results with measured force data of Dickinson et al. (1999) and the fish acceleration data of Walker and Westneat (1997). Ramamurti and Sandberg (2004) have investigated the fluid dynamics underlying the generation of forces during pectoral fin oscillation as fin rigidity is varied.

The results of that work indicated a reduced number of ribs could be used without losing flexibility. The primary objectives of this study are to select the shape of the fin that allows flexibility while keeping the mechanical system less complex and to select the parameters that govern the kinematics of the motion of the fin that maintains thrust for a vehicle in a 3kt current while maintaining the depth within a specified range.

THE INCOMPRESSIBLE FLOW SOLVER

The governing equations employed are the incompressible Navier-Stokes equations in Arbitrary Lagrangian-Eulerian (ALE) formulation which are written as

$$\frac{d\mathbf{v}}{dt} + \mathbf{v}_a \cdot \nabla\mathbf{v} + \nabla p = \nabla \cdot \sigma, \tag{1}$$

$$\nabla \cdot \mathbf{v} = 0, \tag{2}$$

Manuscript approved August 18, 2005.

where p denotes the pressure, $\mathbf{v}_a = \mathbf{v} - \mathbf{w}$ the advective velocity vector, where $\mathbf{v}$ is the flow velocity and $\mathbf{w}$ is the mesh velocity w and the material derivative is with respect to the mesh velocity $\mathbf{w}$. Both the pressure p and the stress tensor σ have been normalized by the (constant) density ρ and are discretized in time using an implicit time stepping procedure. Thus the equations are Eulerian for zero mesh velocity and Lagrangian if the mesh velocity is the same as the flow velocity. The present time-accurate flow solver is discretized in space using a Galerkin procedure with linear tetrahedral elements. The details of the flow solver have already been discussed extensively elsewhere (Ramamurti *et. al.* 1992, 1994, 1995, 1999) in connection with successfully validated solutions for numerous 2-D and 3-D, laminar and turbulent, steady and unsteady flow problems.

RESULTS AND DISCUSSION

Ramamurti and Sandberg (2004) have studied the effect of variable rigidity of the Bird-wrasse fin on the fluid dynamics of force production. The computations showed that when the fin is made rigid by specifying the motion with just the leading edge of the fin tip, the thrust produced during the upstroke is less than half of the peak thrust produced by the flexible cases. During the downstroke, the rigid fin and the fin with the motion prescribed with only the leading and trailing edges produced no positive thrust, while all the flexible cases considered reproduced the thrust production of the fully deformable fin. In the case of the rigid fin, there is a substantial penalty in lift during the upstroke.

Design and Construction

Based on this study, we have reduced the number of ribs for the mechanical fin from 14 spines in the fish to 5 ribs, so as to reduce the complexity of the system while maintaining enough flexibility of the fin surface. The fin was attached to a notional 2ft long Unmanned Underwater vehicle (UUV) having a 4″ diameter cylindrical cross-section (Fig.1), at an angle of attack of α_r at the root of the fin. The fin is flapped at a frequency f with an amplitude ϕ_{max} about the root chord.

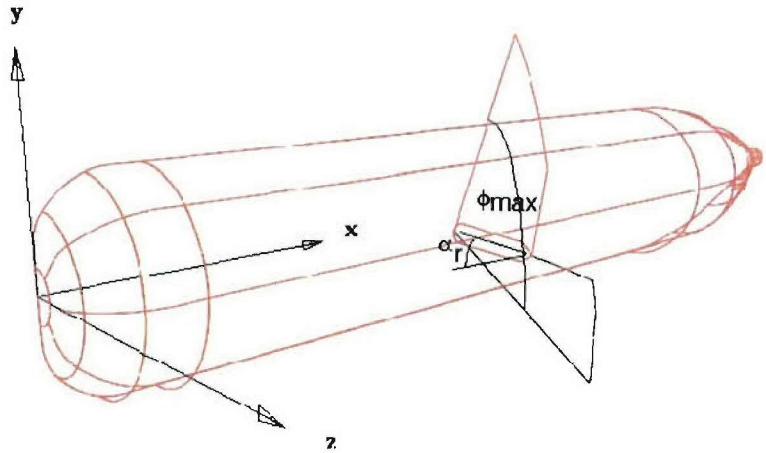

Fig. 1. Schematic of the notional UUV with flapping fin.

The root section of the fin was selected to be of rectangular cross section with rounded leading edges and a tapered trailing edge in order to accommodate the actuators at the base of the ribs. The lengths of the ribs were obtained from the pressure distribution on the fin and from the structural analysis performed by UM researchers. The resulting fin structure is shown in Fig.2. The deforming motion of the fin is obtained by prescribing the motion of the 5 control points or the tips of the ribs (1-5). The kinematics of the ribs is decomposed into two rotations. The first one is a rotation of the all the ribs about the root chord section termed as a bulk or hinge rotation, Fig. 3a, and the second is a supplemental rib rotation which is crucial for the deforming shape of the fin, shown in Fig. 3b. For all the results described, first a steady state solution is obtained using the incompressible flow solver described. From this steady state as initial condition, unsteady flow over several flapping cycles is computed. The motion of the fin is prescribed from the kinematics of the 5 control points. The resulting instantaneous pressure distribution is integrated over the fin and the body surface to yield the thrust and lift forces.

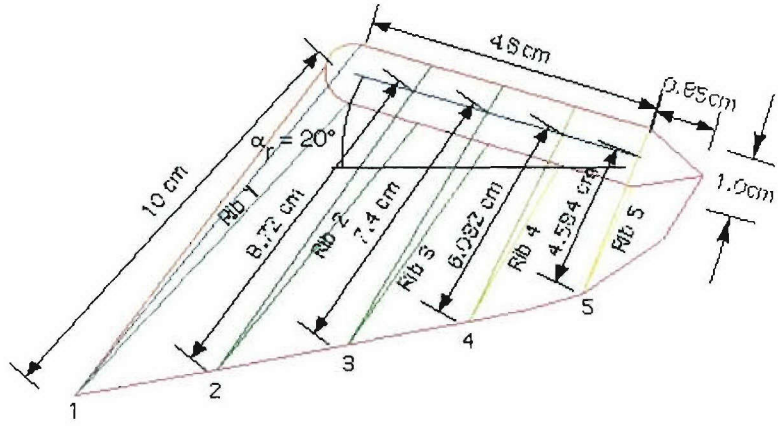

Fig. 2. Schematic of the deforming fin showing the root cross-section and the 5 ribs.

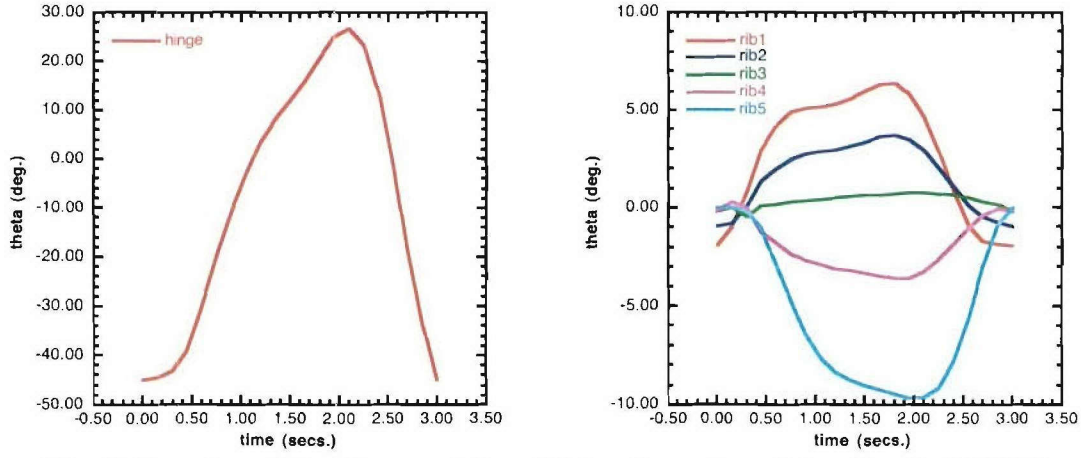

Fig. 3. Rotation of the hinge and the additional rotation of the ribs, $f = 3.333$Hz.

Unsteady Computations

Initially, the fin was oriented to be at an angle $\alpha_r = 30°$ and the flapping amplitude was set to 76°. The position of the beginning of the downstroke is obtained by appropriately scaling the amplitude of the flapping with that of the Bird-wrasse fish and is set to be at –45° about the root/hinge axis. This configuration was first tested for hovering with the fin flapping at frequencies of 0.333Hz and 1.0Hz. The frequencies and the amplitudes were reduced from the fish, which are 3.333Hz and 114°, so that the artificial muscles will be able to generate enough force and respond fast enough. The time history of forces for these cases is shown in Fig. 4 and 5. At $f = 0.333$ Hz, the mean thrust produced is very nearly zero (=-0.008 N), shown in Fig. 4a, implying that the fin produces nearly enough thrust for hovering. Also a mean positive lift is produced at this frequency. As the frequency is increased to 1 Hz, a mean positive thrust of 0.012N and the mean lift is 0.05N. At hovering, as the frequency is increased the thrust production during the upstroke increases sharply. Although the mean lift increases from 0.03N to 0.05N, the range of lift increases almost five fold with increase in frequency.

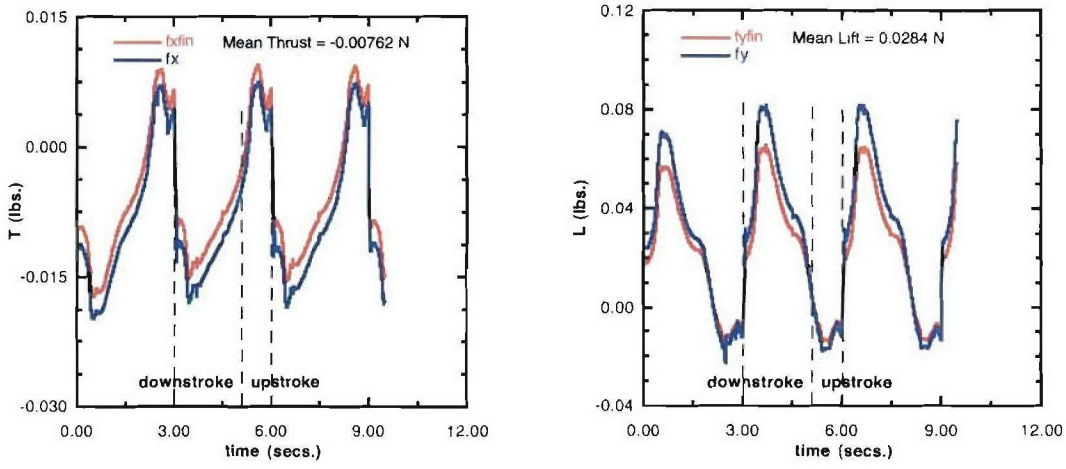

Fig. 4. Thrust and Lift production for a hovering UUV, $f = 0.333$Hz.

The operational requirements for the UUV were set so as to maintain position at a 3kt current. Computations were carried wit incoming velocity set to 3kts. At $f = 0.333$Hz, the current fin configuration produced a drag of 1.342N and a mean lift of 4.023N. The flapping frequency was then increased to 1.0 Hz and the mean drag and lift remained nearly unchanged. The frequency was further increased to 3.333Hz and the mean drag reduced to 1.16N and the mean lift increased to 4.78N. The time history of the force production is shown in Fig. 6. At this flow speed, the current fin configuration and the kinematics is not able to produce enough thrust to maintain position.

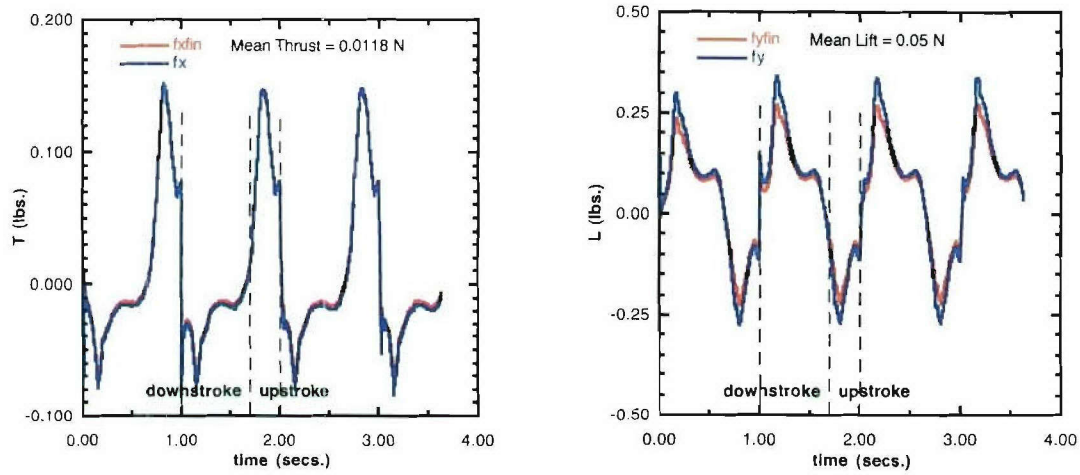

Fig. 5. Thrust and Lift production for a hovering UUV, f = 1.0Hz.

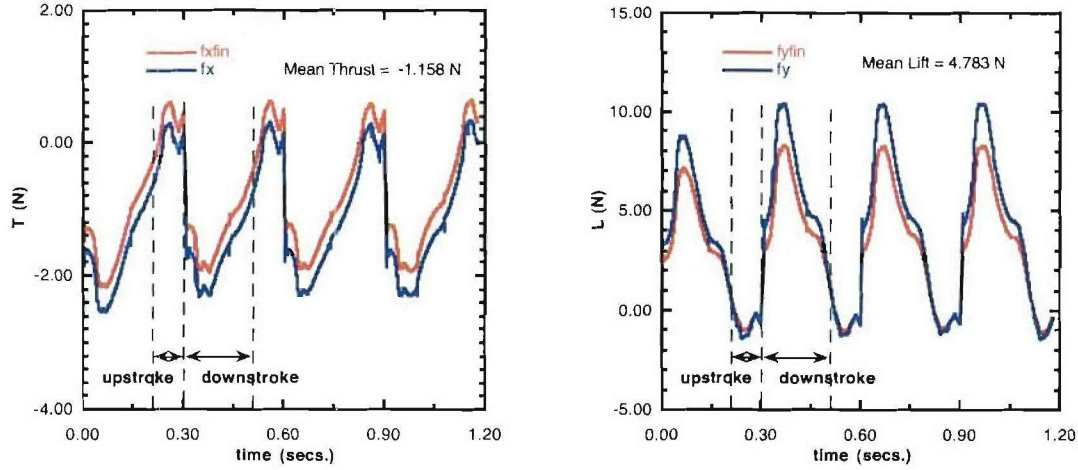

Fig. 6. Thrust and Lift production for a UUV moving at 3kts, f = 3.333Hz.

One of the main differences between the current fin design and the wrasse fin is that the ribs in the present are parallel to each other. This design was chosen to minimize the mechanical complexity. Computationally the ribs can be spread out without much difficulty. Therefore, the trailing edge rib (rib 5) was spread out by 60° with respect to the first or leading edge rib. Computations were carried out at 0.333Hz and the mean drag remained nearly unchanged and is 1.346N, while the mean lift increased to 7.14N. Due to mechanical complexity of spreading the ribs, this option was put aside.

Next, the kinematics of the tips of the leading edge rib (rib1) was modified from the bird-wrasse. Two different methods were attempted to match the kinematics of the fish. First, the spatial slope at the leading edge fin tip, point 1 in Fig2, was matched to that from the wrasse. The slopes at the other control points, 2-5, were retained from the present kinematics. This did not result in any improvement in the thrust. Next, the spatial slope at control points 2-5 were smoothed. Again, the overall men thrust was still negative. The second method is to match the

temporal derivative of the leading control point to that of the wrasse with appropriate scaling for the reduced frequency of 0.333Hz. This also did not result in an improvement in the mean thrust. Few other attempts to reproduce some aspects of the wrasse kinematics such as the maintaining the $\alpha_r = 53°$ or combining a pitching motion of the fin in addition to the flapping did not result in increased thrust. These modifications can be revisited later.

Next, the α_r was changed form 30° to 0°. For this configuration, at $f = 0.333$Hz, the mean thrust improved from –1.342N to –0.7N, Fig. 7a, but the mean lift suffered and reduced from 4.023N to –1.936N, Fig. 7b. As the f increased to 1 Hz, the mean thrust remained nearly the same at –0.65N and with further increase to 3.333Hz, the mean thrust improved to –0.31N, Fig.8a, while the mean lift was nearly –2.0N, Fig. 8b. The loss of lift is due to the lack of positive angle of attack of the fin.

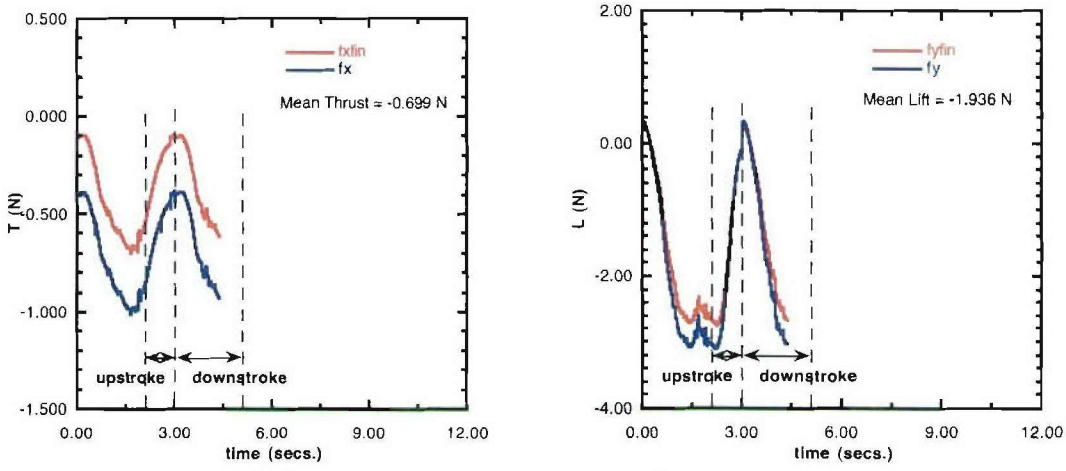

Fig. 7. Thrust and Lift production for a UUV moving at 3kts, $\alpha_r = 0°, f = 0.333$Hz.

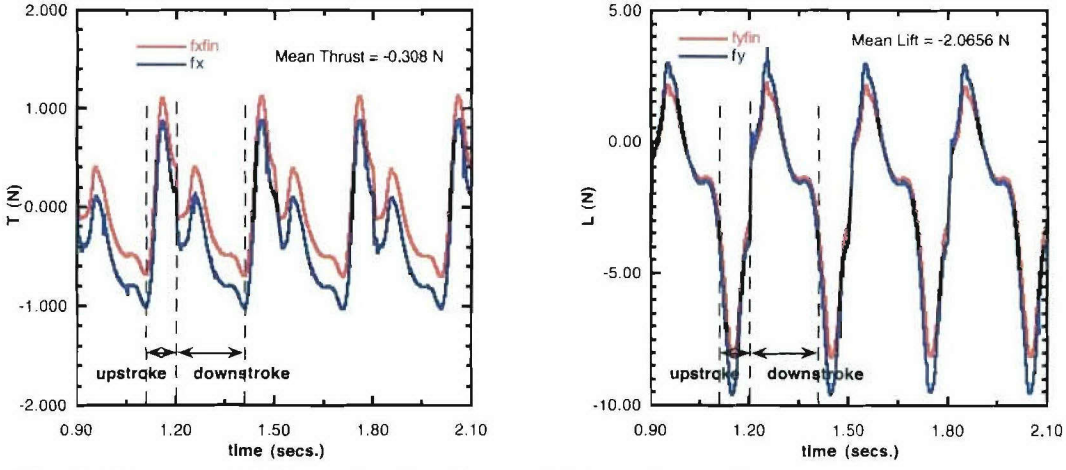

Fig. 8. Thrust and Lift production for a UUV moving at 3kts, $\alpha_r = 0°, f = 3.333$Hz.

Another key parameter that is different from the bird-wrasse is the amplitude of oscillation, which was set to 76° compared to a valued 114° in the fish. Hence, the amplitude was matched

to that of the fish by increasing the rotations of all the ribs. The combined rotation of the ribs and the hinge for this case is shown in Fig. 9. Also, the angle of attack at the root was increased to 10°. The position of the beginning of the downstroke was set to be at –85° about the root-chord axis. At a frequency f= 1.0 Hz, this configuration produced a mean drag of 0.33N and a mean lift of –1.476N. As the frequency is increased to 3.333Hz, a positive mean thrust of 0.264N was produced, but the mean lift remained negative. The results are shown in Fig. 10.

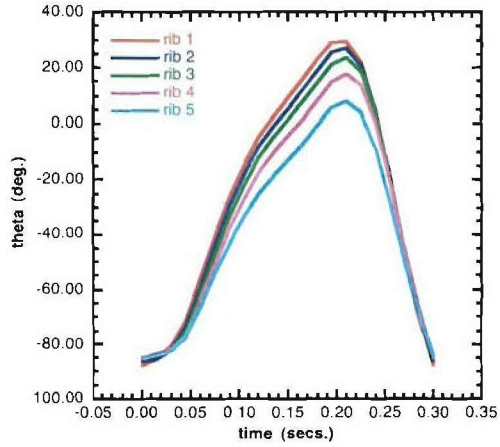

Fig. 9. Rotations of the ribs for increased amplitude, f = 3.333Hz.

As the α_r is further increased to 20°, the thrust and lift generation continued to improve. At f = 1.0Hz, the mean thrust produced is –0.25N and a mean lift of 0.37N was produced, as shown in Fig. 11. At the higher frequency of 3.333Hz, a positive mean thrust and lift of 0.33N and 0.42N, respectively, were produced, as shown in Fig. 12a and b.

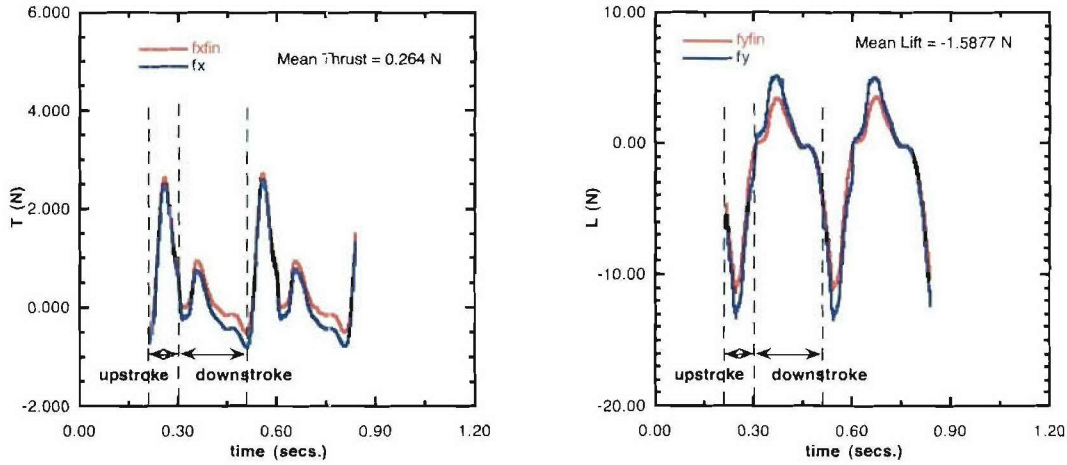

Fig. 10. Thrust and Lift production for a UUV moving at 3kts, α_r = 10°, ϕ_{max} = 114°, f = 3.333Hz.

As the root angle of attack is increased further to 30°, the mean thrust reduced to –0.7N at f = 1 Hz and to –0.2N at f = 3.333Hz. The mean lift was nearly 2.3N for both the frequencies tested. Therefore, it was deemed 20° is near optimal angle of attack of the root. In order to produce a prototype of the fin, it was necessary to increase the spacing between the ribs from 0.8cm to at least 1.2cm.

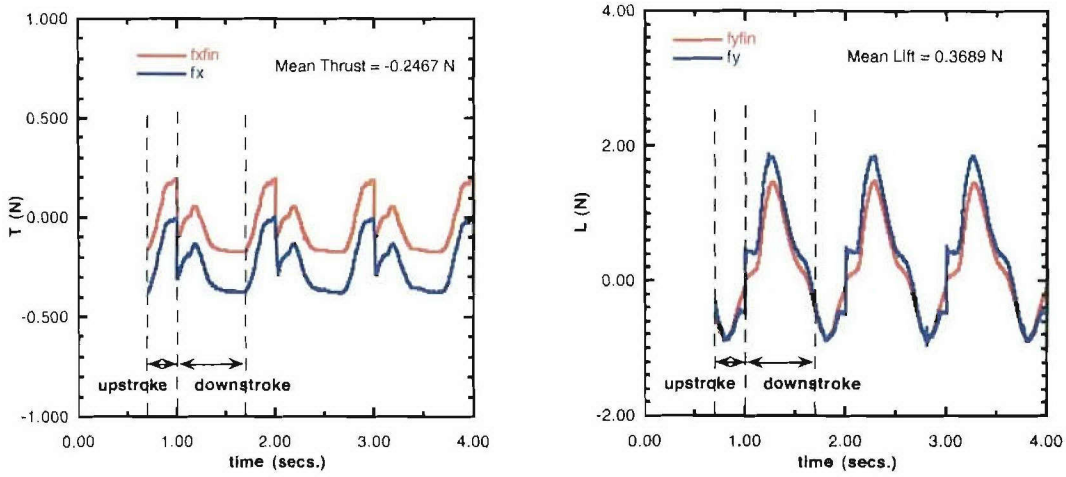

Fig. 11. Thrust and Lift production for a UUV moving at 3kts, $\alpha_r = 20°$, $\phi_{max} = 114°$, $f = 1.0$Hz.

The spacing between the ribs was increased to 2.0cm. At $f = 1.0$Hz, the mean thrust was reduced from –0.25N to –0.63N. In an attempt to recover this lost thrust, the length of the ribs was doubled. This resulted in a positive thrust of 0.49N and the mean lift of 1.49N, Fig. 13. A closer look at lift production showed that the vehicle would undergo large excursions in the vertical direction. The minimum and maximum values of the lift for this case were –14.27 N and +14.04N compared to a value of –0.95N and 1.91N for the case when the rib spacing was 0.8cm and with the original length of the ribs. Therefore, the rib spacing was reduced to minimum possible value of 1.2cm. This resulted in reduction in the thrust produced to a mean value of –0.32N and the mean lift is 0.58 N. The minimum and maximum values of the lift force during the cycle are –0.95N and 2.3N, respectively. Figure 14 shows the time history of force production for this case.

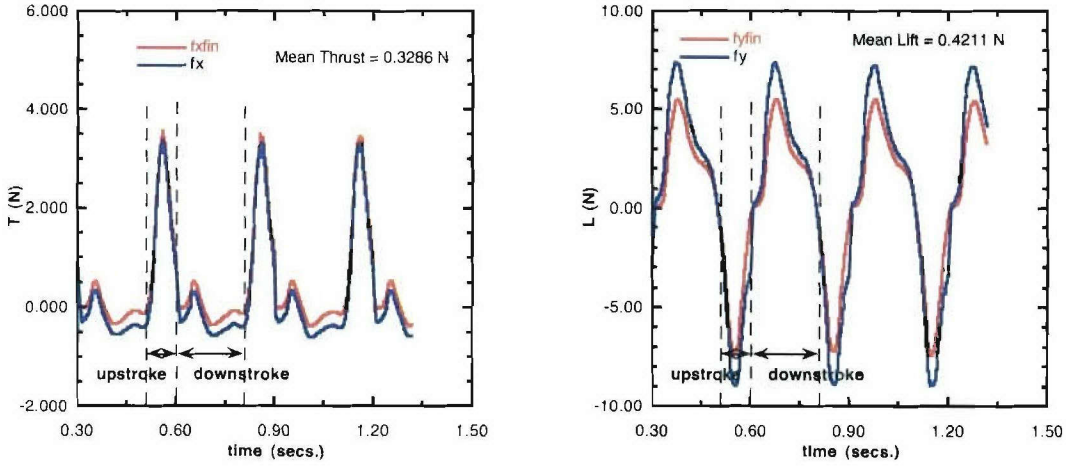

Fig. 12. Thrust and Lift production for a UUV moving at 3kts, $\alpha_r = 20°$, $\phi_{max} = 114°$, $f = 3.333$Hz.

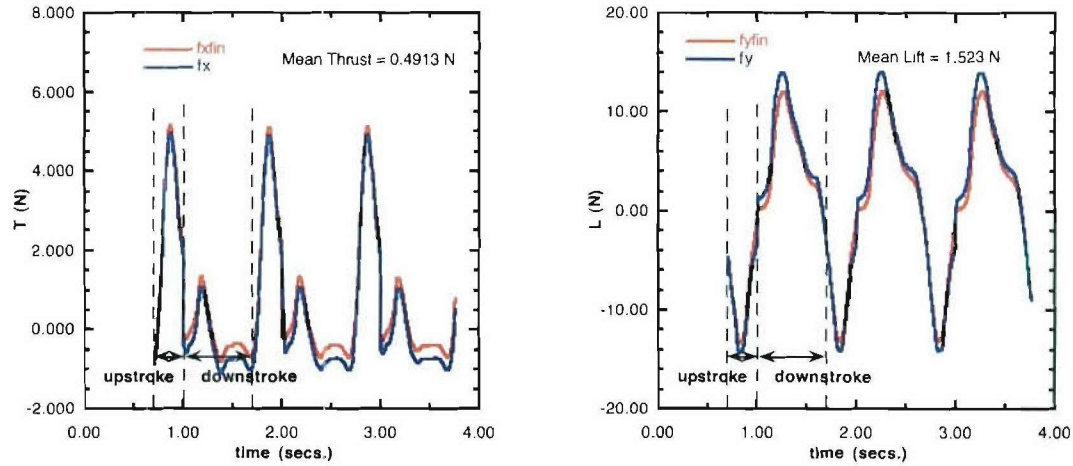

Fig. 13. Thrust and Lift production for a UUV moving at 3kts, $\alpha_r = 20°$, $\phi_{max} = 114°$, $f = 1.0$Hz, rib spacing = 2cm and with doubled rib lengths.

As the rib lengths were increased by a constant factor of 1.5, the mean thrust improved to –0.25N and the mean lift increased to 1.28N. The range of lift force widened to be between –5.68N and 3.22N. In order to add more curvature to the fin, the phasing of the interior ribs 2-4 were modified. This resulted in an improvement in the variation of the lift forces, but the mean thrust reduced to –0.46N.

Another computational experiment was performed to see the effect of a more aerodynamic root section. For this case, a NACA0015 section was chosen with the maximum thickness to be 1cm. The mean thrust remained nearly unchanged from the case shown in Fig. 14 and is -0.35N; the mean lift for this case is 0.95N with the minimum and maximum values of lift at –0.62N and 2.67N. Therefore, the improvement is not significant to warrant a change in the root section that will further complicate the housing of the actuators for the ribs especially near the trailing edge.

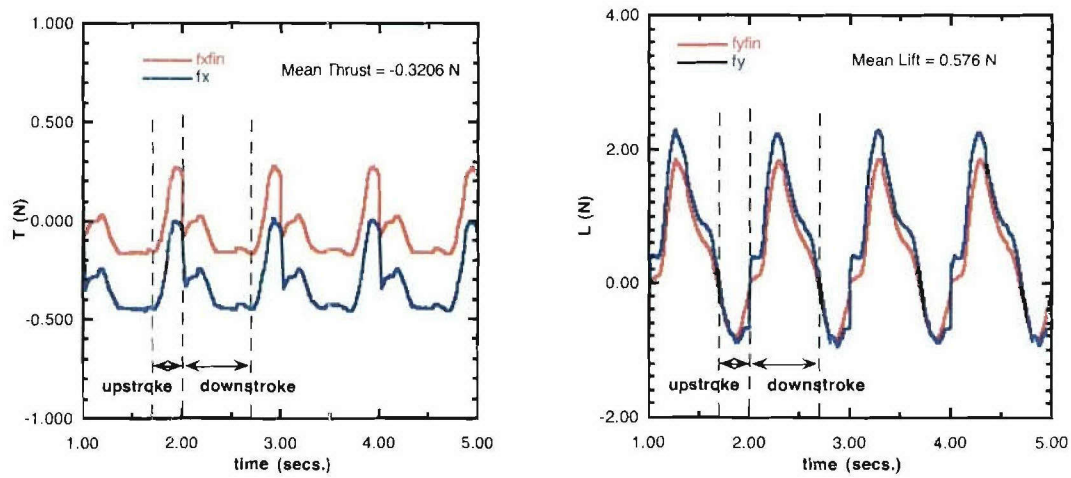

Fig. 14. Thrust and Lift production for a UUV moving at 3kts, $\alpha_r = 20°$, $\phi_{max} = 114°$, $f = 1.0$Hz, rib spacing = 1.2cm and with original rib lengths.

In order to estimate the size of the tank needed to test the prototype fin, an isolated fin was immersed in a 4′ × 2′ × 4′ computational tank. The results of the simulation showed that the force produced by the fin was nearly unchanged and the walls of the tank were not close enough to interfere. This simulation did not take into effect the nearness of the free surface of the water which is beyond the scope of this work.

The frequency of flapping was next increased to 2Hz and the force production is shown in Fig. 15. The mean thrust is nearly zero (-0.06N) implying that the vehicle will be able to sustain a 3kt current. The mean lift for this case is 0.58N with the minimum and maximum values of the lift force at –4.55N and 4.95N, respectively.

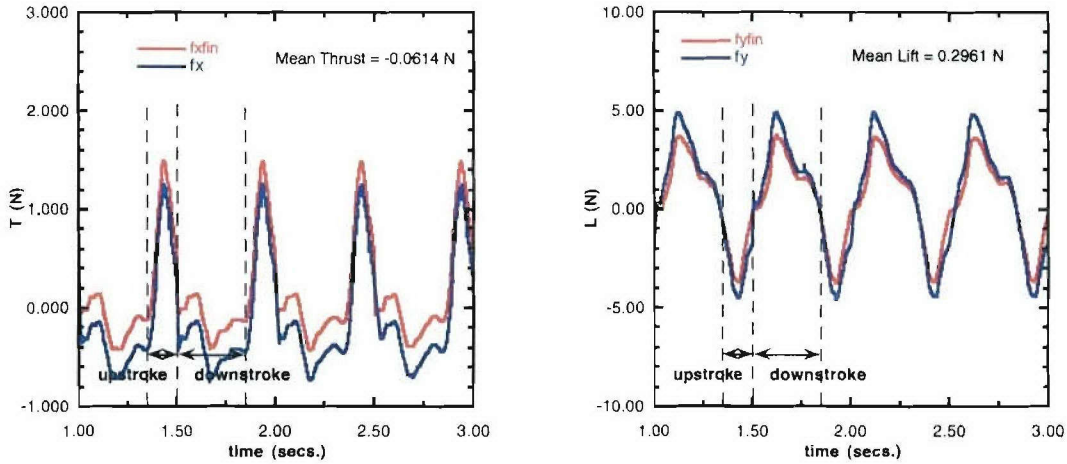

Fig. 15. Thrust and Lift production for a UUV moving at 3kts, $\alpha_r = 20°$, $\phi_{max} = 114°$, $f = 2.0$Hz, rib spacing = 1.2cm and with original rib lengths.

The pressure distribution and the force vector at the instant when the thrust reaches a peak during the upstroke and the downstroke is shown in Fig. 16a-d. During the upstroke high pressure is observed in the upper surface of the fin (Fig. 16b) and a small region on th elower surface near the intersection of the leading edge and the root of the fin (Fig. 16a). Due to the curvature of the fin at this instant, a positive thrust is developed. During the downstroke, high pressure region is present on the lower surface of the fin, producing a positive thrust and a positive lift force. The coordinate system shown in this figure are to orient the fin with respect to the inflow direction and is not the actual location used for computations.

The hydrodynamic power requirement for this configuration was obtained from the force time history and the velocity of the fin. For this purpose, the third cycle of oscillation of the fin, between 1.35 secs. and 1.85 secs. was chosen. The mean power required during the cycle is 1.573 Watts which translates to an energy consumption of 0.79 Joules/cycle. The inertial power required to move the fin can be obtained from the moment of inertia of the fin, the angular acceleration of the hinge rotation and the angular velocity of the hinge. The mean inertial power required to move the fin assuming unit specific gravity for the fin is 0.1W. These power requirements are shown in Fig. 17.

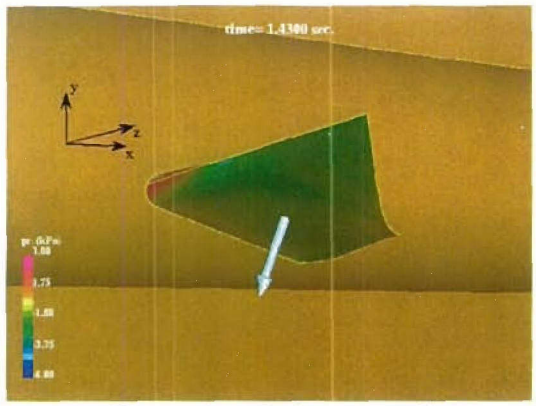

a. front view during upstroke

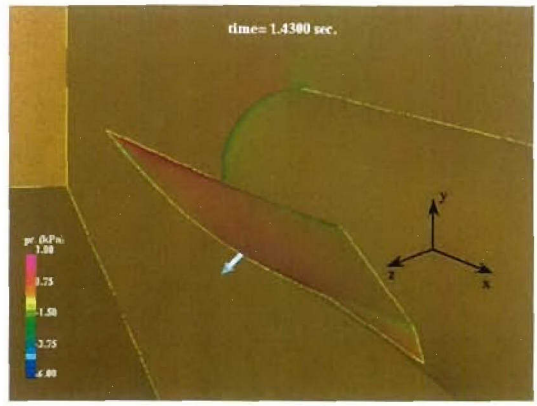

b. top view during upstroke

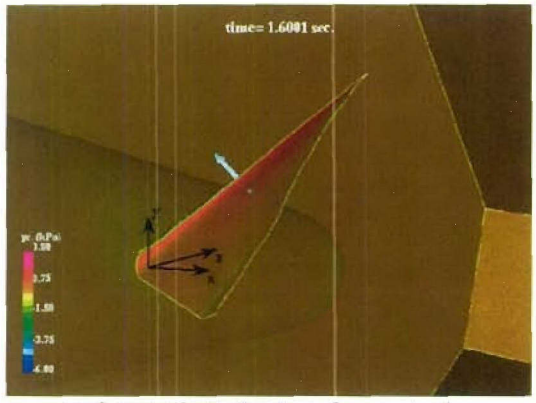

c. front view during downstroke

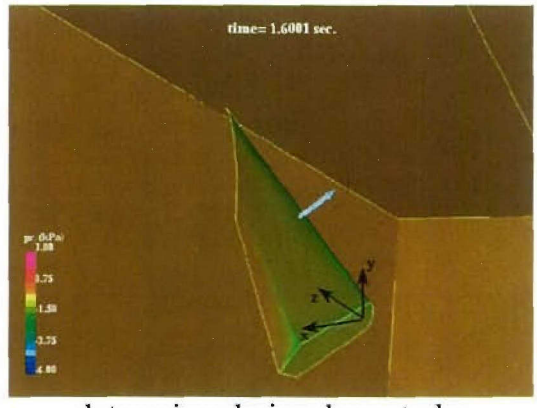

d. top view during downstroke

Fig. 16. Pressure distribution on the fin at maximum thrust production instants.

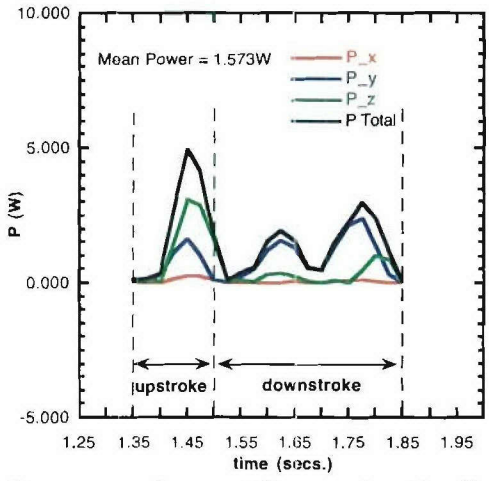

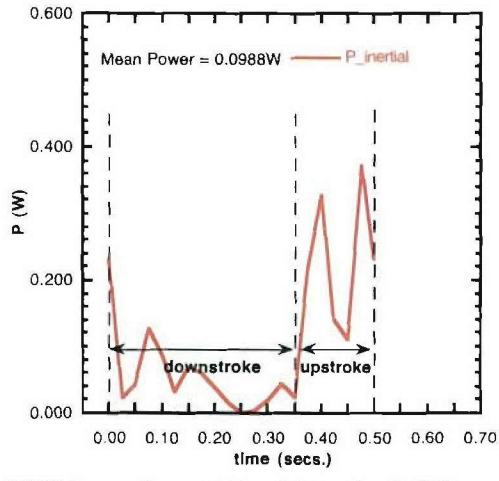

Fig. 17. Power requirement for moving the fin for a UUV moving at V = 3kts, f = 2.0Hz, (a) Hydrodynamic, (b) Inertial.

SUMMARY AND CONCLUSIONS

The 3-D unsteady computations of a notional UUV with a flapping fin have been carried out. Several parameters in the design of the flapping fin have been varied. Based on our previous study on the effect of rigidity of the Bird-wrasse fin on the force production in fishes, the number of ribs for the current flapping fin is reduced to 5. This is done in order to reduce the complexity of the mechanical system. The important parameters that govern the thrust production are the angle of attack of the root section of the fin, the frequency and the amplitude of flapping. After several parametric studies varying the angle of attack of the root section of the fin, it was found that 20° was near optimum. The original NRL-UM kinematics was also modified so that the amplitude of the oscillation is 114°and a frequency of 1Hz. The rib spacing was set to the minimum possible value of 1.2cm, from mechanical constraints. This resulted in reduction in the thrust produced to a mean value of –0.32N and the mean lift is 0.58 N. The minimum and maximum values of the lift force during the cycle are –0.95N and 2.3N, respectively. As the frequency of oscillation is increased from 1 Hz to 2Hz, the mean thrust is nearly zero (-0.06N) implying that the vehicle will be able to sustain a 3kt current. The mean lift for this case is 0.58N with the minimum and maximum values of the lift force at –4.55N and 4.95N, respectively. The hydrodynamic power requirement for this configuration was obtained from the force time history and the velocity of the fin. The mean power required during the cycle is 1.573 Watts which translates to an energy consumption of 0.79 Joules/cycle.

ACKNOWLEDGEMENTS

This work was supported by ONR through an NRL 6.2 project: "Unsteady Hydrodynamics of Swimming Vehicles." The valuable weekly discussions with Dr. B.R. Ratna and Dr. C. Spillman are greatly appreciated. This work was supported in part by a grant of HPC time from the DoD HPC centers, ARL MSRC SGI-O2K and NRL SGI-O2K.

REFERENCES

Dickinson, M. H., Lehmann, F.-O. and Sane, S. P. (1999). Wing rotation and the aerodynamic basis of insect flight. *Science* **284**, 1954-1960.

Ellington, C. P., Van den Berg, C. and Willmott, A. P. (1996). Leading-edge vortices in insect flight. *Nature* **384**, 626-630.

Liu, H. and Kawachi, K. (1998). A numerical study of insect flight. *J. comp. Physics.* **146**, 124-156.

Ramamurti, R. and Löhner, R. (1992). Evaluation of an Incompressible Flow Solver Based on Simple Elements, *Advances in Finite Element Analysis in Fluid Dynamics*, FED **137**, Editors: Dhaubhadel, M. N. *et al.*, ASME Publication, New York, 33-42.

Ramamurti, R. and Sandberg, W.C. (2002a). A Three-Dimensional Computational Study of the Aerodynamic Mechanisms of Insect Flight, *J. Exp. Biol.* **205**, 1507-1518.

Ramamurti, R., Löhner, R., and Sandberg, W. C. (1994). Evaluation of a Scalable 3-D Incompressible Finite Element Solver, *AIAA-94-0756*, Washington, DC.

Ramamurti, R., Löhner, R., and Sandberg, W. C. (1995). Simulation of a Torpedo Launch Using a 3-D Incompressible Finite Element Flow Solver, *AIAA-95-0086*, Washington, DC.

Ramamurti, R., Löhner, R., and Sandberg, W. C. (1999). Computation of the 3-D Unsteady Flow Past Deforming Geometries, *Int. J. Comp. Fluid Dyn.*, 13, 83-99.

Ramamurti, R., Sandberg, W.C. and Löhner, R. (2000). Simulation of the Dynamics of Micro Air Vehicles, *AIAA-2000-0896*, Reno, NV.

Ramamurti, R., Sandberg, W.C., Löhner, R., Walker, J. A. and Westneat, M. W. (2002b). Fluid Dynamics of Flapping Aquatic Flight in the Bird Wrasse: 3-D Unsteady Computations with Fin Deformation, *J. Exp. Biol.* **205**, 19, 2997-3008.

Walker, J. A. and Westneat, M. W. (1997). Labriform Propulsion in Fishes: Kinematics of Flapping Aquatic Flight in the Bird Wrasse, *Gomphosus Varius*. (Labridae), *J. Exp. Biol.* **200**, 1549-1569.

Willmott, A.P. and Ellington, C.P. (1997). The mechanics of flight in the hawkmoth Manduca Sexta. II. Aerodynamic consequences of kinematics and morphological variation, *J. Exp. Biol.* **200**, 2723-2745.